Int. J. Electrochem. Sci., 13 **(2018)** 11502 – 11515, doi: 10.20964/2018.12.07

International Journal of
ELECTROCHEMICAL
SCIENCE
www.electrochemsci.org

Corrosion Behaviour and Electrochemistry of Mg-5Y-2Nd-0.5Zr-*x*Sm (*x*=0, 1, 3 and 5) Alloys in 3.5 wt.% NaCl

Yunwei Gui[1], *Quanan Li*[1, 2,*], *Jun Chen*[1], *Qing Zhang*[1], *Sanling Fu*[1], *Limin Zhu*[1]

[1] School of Materials Science and Engineering, Henan University of Science and Technology, Luoyang 471023, China
[2] Collaborative Innovation Center of Nonferrous Metals, Henan Province, Luoyang 471023, China
[*]E-mail: guiyunwei1@163.com

Received: 9 July 2018 / *Accepted:* 23 September 2018 / *Published:* 5 November 2018

The effects of Sm on the corrosion behaviours and electrochemistry of Mg-5Y-2Nd-0.5Zr magnesium alloy were studied by the static weight loss method, electrochemical analysis, scanning electron microscopy and XRD. The results showed that the addition of Sm increased the open circuit potentials of the tested alloys, decreased their self-corrosion current densities, and improved their corrosion resistances. As the Sm content increased, the corrosion rate of the alloy first decreased and then reached a minimum at 3 wt.% Sm. At 3 wt.% Sm content, the corrosion rate of the alloy decreased to 0.2121 $mg.cm^{-2}.h^{-1}$, which was 57% of that of the original alloy. At the same time, the Sm formed a new $Mg_{41}Sm_5$ phase in the alloy, which changed the quantities and distributions of the second phases in the Mg-5Y-2Nd-3Sm-0.5Zr alloy. Adding a proper amount of Sm refines the precipitates and makes the components and tissues uniform. The uniform, fine second phases could provide a good barrier against the generation and expansion of corrosion, thereby significantly improving the corrosion resistance of the alloy.

Keywords: Mg-Y-Nd-Sm alloy, Sm, Second phases, Corrosion resistance, Electrochemistry

1. INTRODUCTION

Magnesium alloys are lightweight, have high specific stiffnesses, high damping, remarkable shock absorption and noise reduction, good electrical and thermal conductivities and are widely used in the transportation, communications, aerospace and other fields[1-6]. However, due to the poor corrosion resistances of magnesium alloys, their further promotion and application are limited[2-9]. Improving the corrosion resistances of magnesium alloys has become a hot topic in the field of materials research. Studies have shown that rare earth elements and mixed rare earths affect the corrosion properties of magnesium alloys[4-11]. The effects of La, Ce and Y on the corrosion resistance of magnesium alloys have been studied, and the corrosion resistance of magnesium alloys

has been improved to varying degrees[5-16]. At present, the mechanisms of the influence of Sm on the properties of magnesium alloys need further study.

Sm has a high solid solubility in a Mg matrix and can reach 5.8 wt.%. In addition, Sm_2O_3 has the lowest price among the single rare earth oxides, which is expected to greatly reduce the costs of Sm-containing alloys[7-19]. Sm has broad application prospects in Mg alloys. On this basis, we chose to replace a portion of the Nd in a more mature commercial WE series (Mg-4Y-3Nd-0.5Zr and Mg-5Y-4Nd-0.5Zr alloys) magnesium alloy with the more solid-soluble Sm, developing new Mg-5Y-2Nd-*x*Sm-0.5Zr (*x*=0, 1, 3, 5) alloys with lower costs and superior mechanical properties[20]. However, no research exists regarding the corrosion resistance and electrochemical performance of Sm in the Mg-5Y-2Nd-*x*Sm-0.5Zr (*x*=0, 1, 3, 5) alloys. In this paper, the effects of rare earth Sm on the corrosion resistances and electrochemistry of Mg-5Y-2Nd-*x*Sm-0.5Zr (*x*=0, 1, 3, 5) alloys[20] were studied by weight loss corrosion and electrochemical methods, and the optimal amount of Sm for a Mg-Y-Nd magnesium alloy was determined.

2. EXPERIMENTS

2.1 Materials

The raw materials used in the experiments were pure magnesium ingot (99.98 wt.%) and intermediate alloys Mg-30Y, Mg-30Nd, Mg-30Sm and Mg-30Zr (mass fraction, %). Alloys with compositions of Mg-5Y-2Nd-*x*Sm-0.5Zr (wt.%) *x*=0, 1, 3, 5 were formed through a melt process. All raw materials were dried before installation in the furnace. The alloy smelting was carried out in a type ZG.JL0.01-40-4 electromagnetic medium frequency induction furnace using a high-purity corundum crucible. During the smelting process, a mixture of SF_6 and CO_2 at a volume ratio of 1:99 was introduced for protection. The alloy was melted, stirred and allowed to stand. When the alloy had cooled to 700 ℃-710 ℃, it was poured into a steel mould that had been preheated to 250 ℃. The alloy test piece obtained was covered with MgO powder and heat-treated in a box-type electric resistance furnace. The heat treatment process for the alloy was solid solution (heating at 525 ℃ for 10 h and then water quenching at 80 ℃) and ageing (heating at 225 ℃ for 12 h and then air cooling).

2.2 Corrosion experiments

The alloys were cut into cubes sized 10 mm × 10 mm × 10 mm using a wire cutting device. After grinding all the surfaces of the samples with 2000-grit sandpaper, they were cleaned with alcohol. The samples were soaked in 3.5 wt.% NaCl solution for 24 h and then placed in a 20% CrO_3 + 1% $AgNO_3$ solution at 90 °C for 10 min to clean the corrosion products. The mass of the sample before and after corrosion was measured on an analytical balance, and the corrosion rate of the alloy was calculated according to formula (1):

$$c = \frac{(m_0 - m)}{ST} \quad (1)$$

where c is the corrosion rate, m_0 is the mass of the alloy before corrosion, m is the mass of the

alloy after corrosion, *S* is the surface area of the alloy, and *T* is the corrosion time.

2.3 Electrochemical experiments

The electrochemical performances of the alloys were tested by a CHI660E electrochemical workstation. A three-electrode system was used where the counter electrode was a graphite electrode, the auxiliary electrode was a saturated calomel electrode (SCE), and the sample and the auxiliary electrode were connected by a salt bridge. Each test specimen had a working area of 1 cm^2. After the open circuit potential (OCP) stabilized, an AC impedance test was conducted. The frequency test range was 10^5-10^{-1} Hz, and the voltage amplitude was 5 mV. Then, the polarization curve of the sample was measured, and the constant potential scanning method was used. The scan range was -2 to -1 V, and the scan rate was 1 mV/s.

2.4 Analysis and characterization methods

The microstructure of the Mg-5Y-2Nd-*x*Sm-0.5Zr alloy was characterized by scanning electron microscopy (JSM-5610LV). The alloy was subjected to EDS spectroscopy and X-ray diffraction spectroscopy (D8 ADVANCE) analysis to determine the phases present; the XRD experimental conditions were as follows: a Cu Kα source, scan angle from 15°~90°, and scan speed of 2°/min. When the immersion tests were complete, the corrosion products on the surface of different samples were calibrated and analysed by XRD. The corrosion surface topographies of the samples with the corrosion products removed were observed by SEM (JSM-5610LV).

Table 1. Chemical compositions of the Mg-5Y-2Nd-*x*Sm-0.5Zr alloys (wt.%) (*x*=0, 1, 3, 5) as determined by ICP.

Nominal composition	Actual composition (wt.%)				
	Y	Nd	Sm	Zr	Mg
Mg-5Y-2Nd-0.5Zr	5.13	2.04	0	0.53	Bal.
Mg-5Y-2Nd-**1Sm**-0.5Zr	4.95	1.92	1.12	0.56	Bal.
Mg-5Y-2Nd-**3Sm**-0.5Zr	5.07	2.11	3.09	0.45	Bal.
Mg-5Y-2Nd-**5Sm**-0.5Zr	5.21	2.09	4.97	0.47	Bal.

3. RESULTS AND DISCUSSION

3.1 The microstructure of samples

Fig. 1 shows the X-ray diffraction analyses of the aged Mg-Y-Nd-Sm-Zr alloys. The analysis results show that the main phases of the Mg-5Y-2Nd-0.5Zr alloy are the α-Mg, $Mg_{24}Y_5$ and $Mg_{41}Nd_5$

phases. With the addition of Sm, a new $Mg_{41}Sm_5$ phase is produced, and at the same time, the characteristic diffraction peak for the $Mg_{41}Nd_5$ phase becomes increasingly prominent. These results show that the addition of Sm promotes the precipitation of the $Mg_{41}Nd_5$ phase. Therefore, Sm atoms and Nd atoms can replace each other in the β' phase (β'-$Mg_{41}Nd_5$) crystal structure precipitated over the ageing time, making the phase composition more complicated[11-26].

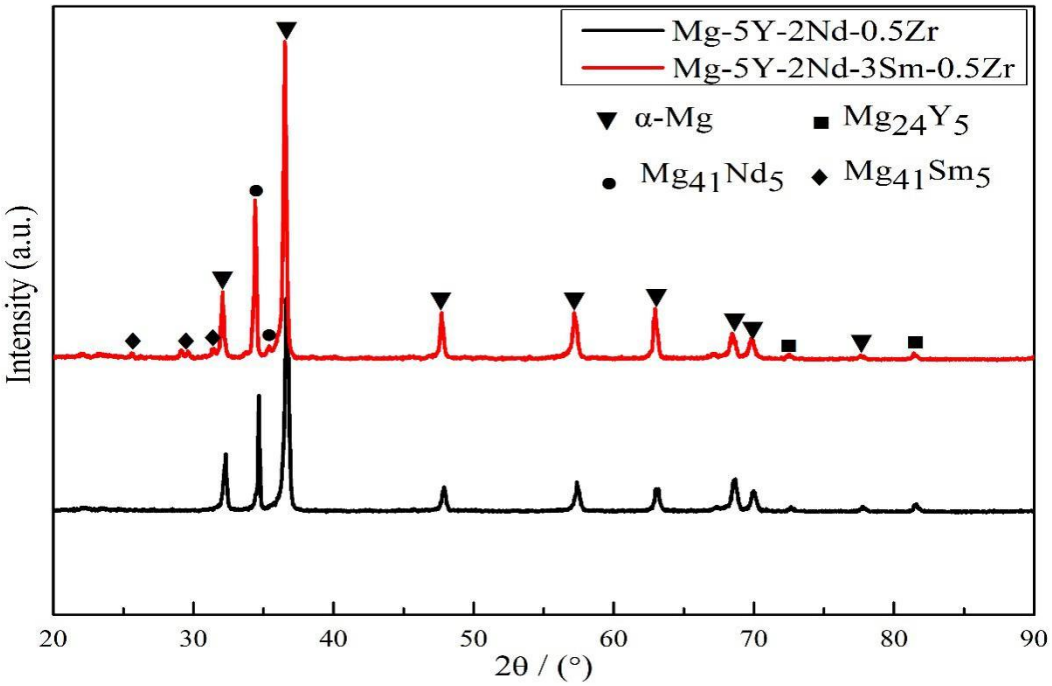

Figure 1. X-ray diffraction spectra of peak-aged Mg-5Y-2Nd-*x*Sm-0.5Zr alloys (*x*=0, 3) (wt.%).

Fig. 2 and Table 2 show SEM images and EDS analysis results, respectively, for four aged Mg-Y-Nd-Sm-Zr alloys. Table 2 shows that Mg, Y, Nd and Zr are detected in the alloys without rare earth Sm additions. As can be seen in Fig. 2, the alloy essentially consists of black α-Mg matrix and white second phases. The Mg-5Y-2Nd-0.5Zr alloy mainly accumulates coarse second phases, which is shown in Fig. 2(a). With the addition of Sm, a new, fine-grained second phase with a relatively uniform distribution appears in the alloy, as shown in Figures 4(b)-(d). As the Sm content increases, the number of second phases gradually increases. When the amount of Sm reaches 5%, a continuous network distribution occurs. According to the analysis of EDS spectra from different forms of the white second phase as shown in Table 2, the mass fraction of Sm in the eutectic phase increases with increasing Sm content, and the mass fractions of Y and Nd decrease. The amount of the compound containing Sm increases. At the same time, the relatively fine grained second phase distributed in the grains inside the alloy consists mainly of regions rich in Y, Nd, or Sm. Combined with the XRD calibration in Fig. 1, we can infer that the fine grained second phase comprises a mix of $Mg_{24}Y_5$, $Mg_{41}Nd_5$ and $Mg_{41}Sm_5$ phases. When Sm is added, the Sm displaces a portion of the Y and Nd, dissolves in the α-Mg matrix, promotes the precipitation of the second phase containing Y and Nd, and changes the alloy morphology and the distributions of the second phases [13-27].

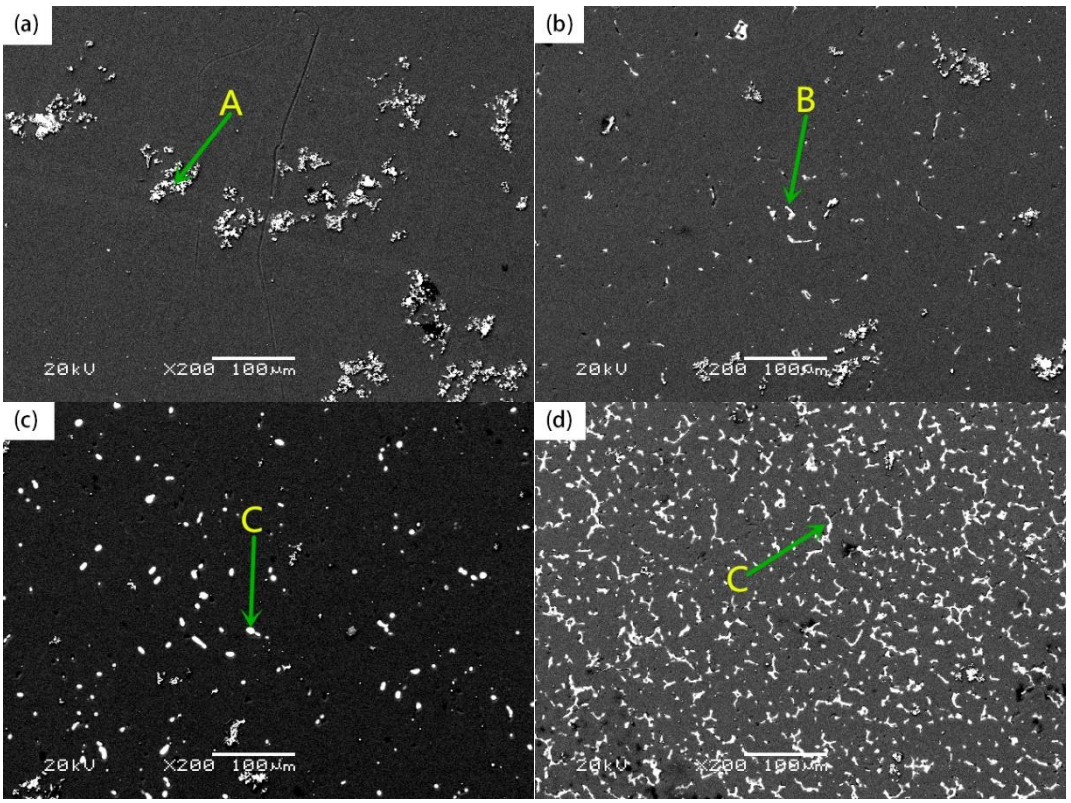

Figure 2. SEM morphologies of peak-aged Mg-5Y-2Nd-*x*Sm-0.5Zr alloys (wt.%) before corrosion: (a) *x*=0, (b) *x*=1, (c) *x*=3 and (d) *x*=5.

Table 2. EDS results for the points marked in Figure 2 (wt.%).

Elements (wt.%)	*x*(Mg)/%	*x*(Y)/%	*x*(Nd)/%	*x*(Sm)/%	*x*(Zr)/%
Figure 2(a), A	44.14	25.29	11.81	—	18.76
Figure 2(b), B	42.14	14.12	13.55	23.97	6.22
Figure 2(c), C	34.31	16.71	12.23	36.54	00.21
Figure 2(d), D	20.56	13.79	16.97	47.03	01.65

3.2 Weight loss rates

Fig. 3 shows the average corrosion weight loss rates of the Mg-5Y-2Nd-*x*Sm-0.5Zr alloys after soaking for 24 h in 3.5 wt.% NaCl solution at 25℃. This figure shows that as the Sm content increases, the corrosion rate first decreases and then reaches a minimum at 3 wt.% Sm, which indicates the best corrosion resistance. When the Sm content is greater than 3 wt.%, the corrosion rate sharply increases. This increase may occur due to an excessive amount of Sm consuming the α-Mg matrix, which results in a decrease in the Mg content, and magnesium-poor regions have decreased corrosion resistance. The alloy series in increasing order of corrosion resistance is 0 wt.% Sm, 1 wt.% Sm, 5 wt.% Sm, and 3 wt.% Sm, and a proper amount of Sm can improve the alloy corrosion resistance. The weight loss rate of the Mg-5Y-2Nd-3Sm-0.5Zr alloy in the corrosive medium is the lowest, which indicates that this content of Sm is the most beneficial for the corrosion resistance of the alloy. This

result is mainly due to the fine grained second phases dispersed in the matrix, which can block the generation and expansion of corrosion and improve the corrosion resistance of the Mg-5Y-2Nd-3Sm-0.5Zr alloy[11-29].

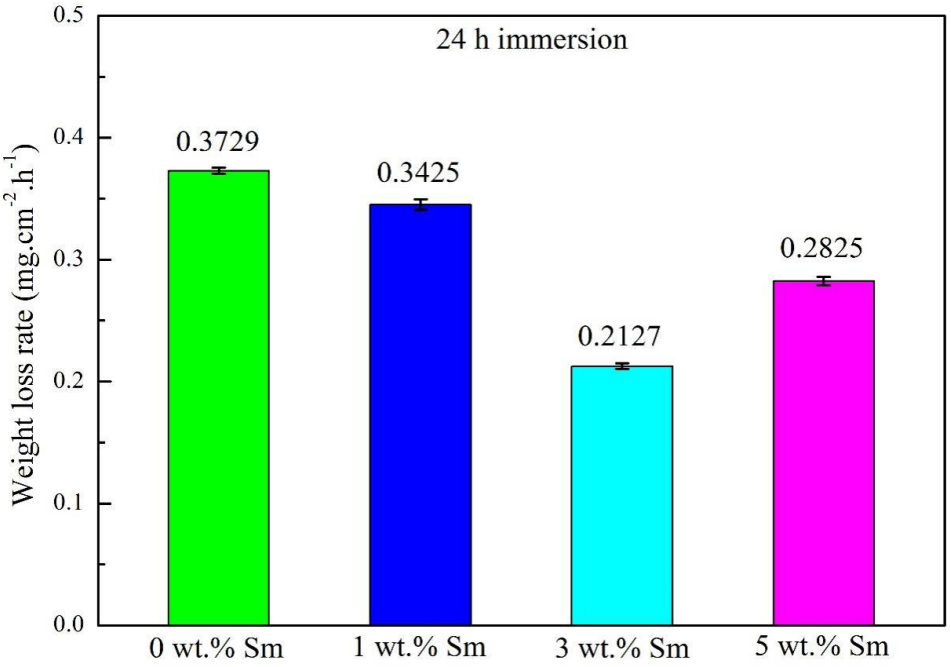

Figure 3. Weight loss rates for the peak-aged Mg-5Y-2Nd-*x*Sm-0.5Zr alloys (*x*=0, 1, 3, 5) (wt.%) after 24 h of immersion in 3.5% NaCl solution.

3.3 Corrosion products and surface morphologies

3.3.1 Corrosion products

To further study the effects of Sm on the corrosion resistance of the Mg-5Y-2Nd-*x*Sm-0.5Zr alloys, the corrosion products on the surface of the alloys were analysed by XRD. No significant differences are found in the corrosion products of the alloys with different Sm contents. The corrosion products are mainly composed of $Mg(OH)_2$ (see Fig. 4). Magnesium alloys are unstable and are susceptible to corrosion. First, MgO is formed in the surface layer. MgO becomes $Mg(OH)_2$ after immersion for a long time by:

$$MgO+H_2O \rightarrow Mg(OH)_2 \quad (2)$$

$$Mg(OH)_2+2Cl^- \rightarrow MgCl_2+2OH^- \quad (3)$$

In addition, only a very small amount of compounds containing rare earth Sm are found in the corrosion products of the alloy. This result indicates that the second phase containing Sm in the alloy has good corrosion resistance[16-28].

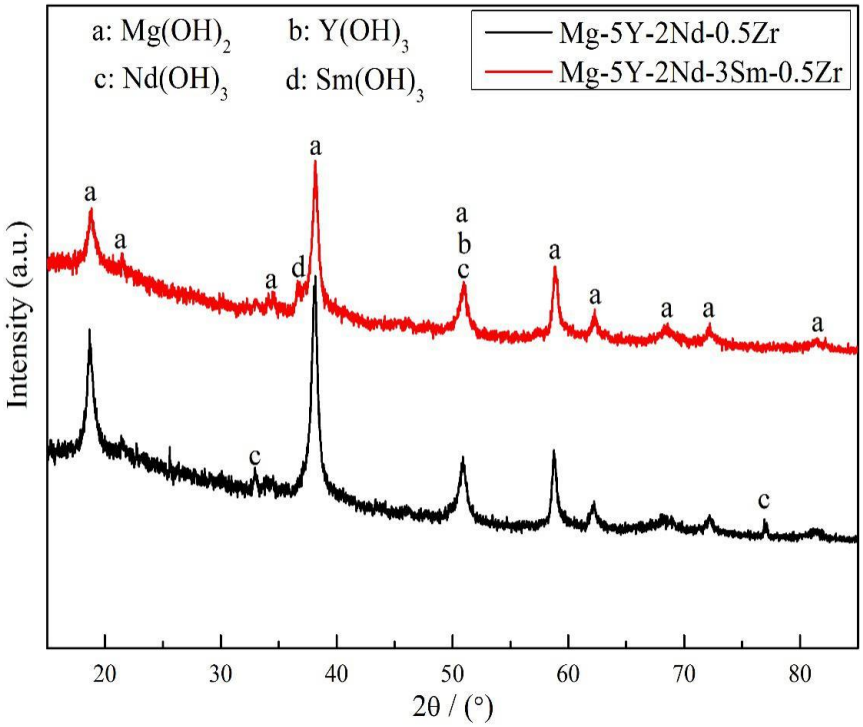

Figure 4. XRD of corrosion products formed on peak-aged Mg-5Y-2Nd-*x*Sm-0.5Zr alloys (*x*=0, 3) (wt.%) after 24 h of immersion in 3.5% NaCl solution.

3.3.2 Corrosion product surface morphologies

Fig. 5 shows the corrosion morphologies of the Mg-5Y-2Nd-*x*Sm-0.5Zr alloys immersed in 3.5 wt.% NaCl solution for 24 hours. Fig. 5 shows that as the Sm content increases, the degree of corrosion in the alloy first decreases and then increases. For the alloy without Sm, the entire surface of the alloy is corroded, the size of the corroded particles is not uniform, and corrosion pits appear in some areas (see Fig. 5(a)). When the Sm content is 3 wt.%, the alloy is slightly corroded, the particles of the scale are small, and only a few points appear (see Fig. 5(c)). As the Sm content further increases, the degree of corrosion becomes severe. These corrosion patterns are consistent with the corrosion rate test results (see Fig. 3).

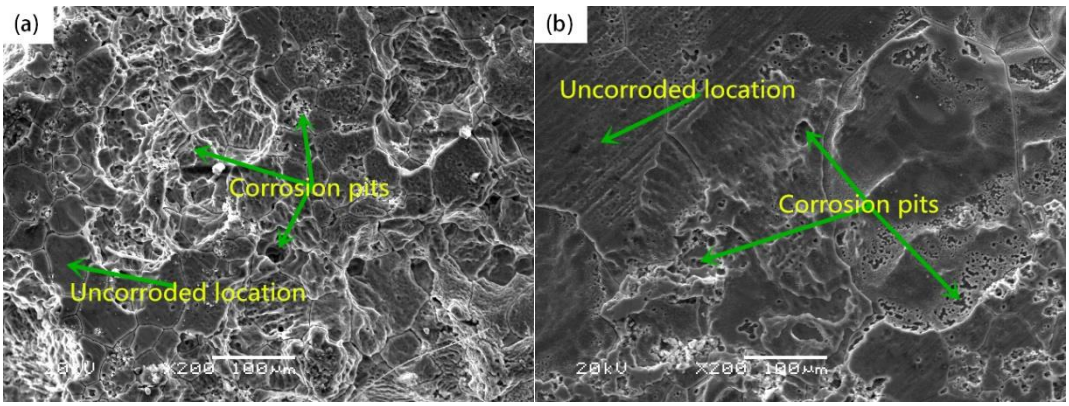

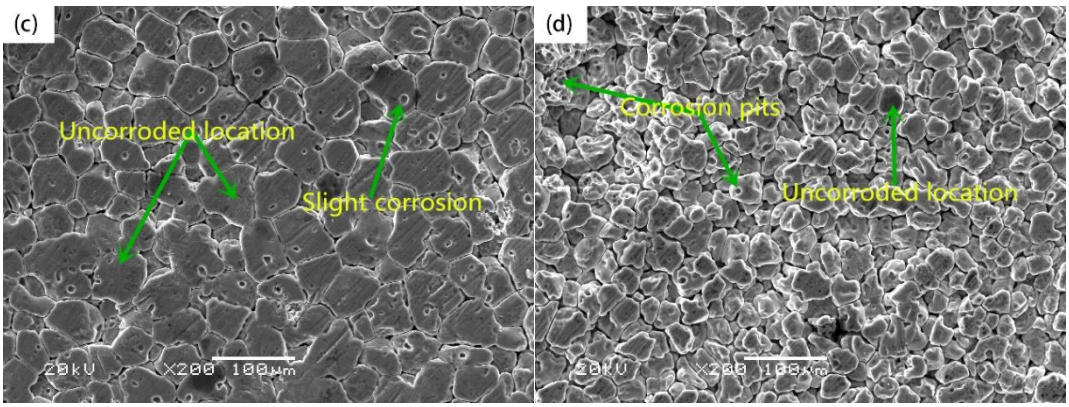

Figure 5. Surface morphologies with corrosion products removed for peak-aged Mg-5Y-2Nd-*x*Sm-0.5Zr alloys (wt.%) after 24 h immersion in 3.5% NaCl solution: (a) *x*=0, (b) *x*=1, (c) *x*=3 and (d) *x*=5.

3.4 Electrochemical characterizations

3.4.1 Open circuit potential test

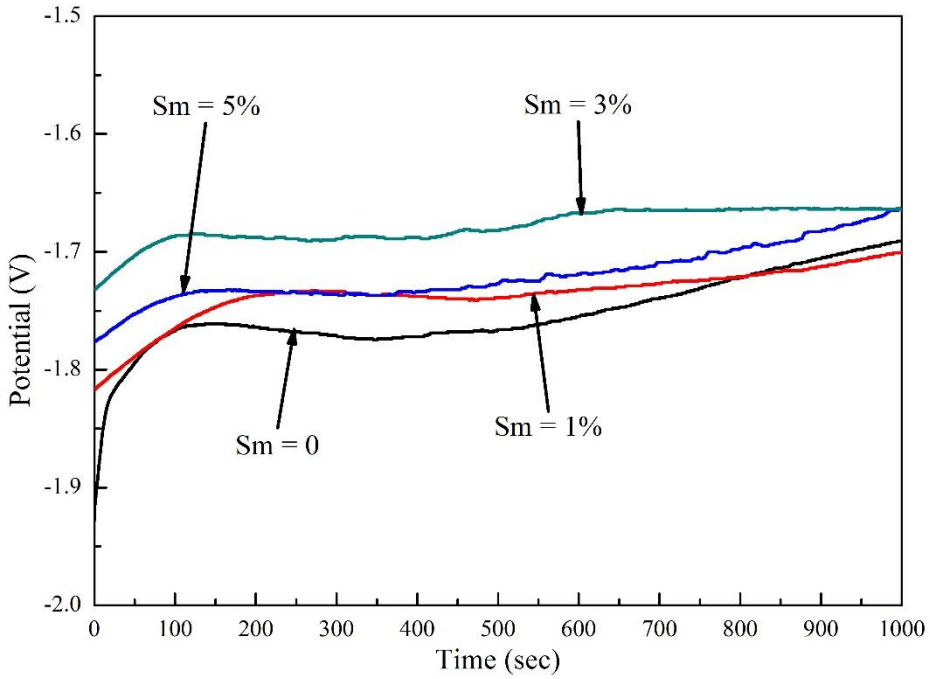

Figure 6. Open circuit potential (OCP) curves for peak-aged Mg-5Y-2Nd-*x*Sm-0.5Zr alloys (*x*=0, 1, 3, 5) (wt.%) in 3.5% NaCl solution.

Fig. 6 shows the open circuit potential curves for the Mg-5Y-2Nd-*x*Sm-0.5Zr alloys in 3.5 wt.% NaCl solution. First, the open circuit potential has the same trend with time, then fluctuates with time, and finally fluctuates around a certain value. The Mg-5Y-2Nd-*x*Sm-0.5Zr alloys are immersed in 3.5% NaCl solution, and the chemical reaction begins. The surface of the magnesium alloy dissolves to form MgO and $Mg(OH)_2$ products, covering the surface of the magnesium metal, which partially hinders the magnesium dissolution and results in a positive shift in the open circuit potential. When the

solution contains Cl^-, the surface corrosion products adsorb Cl^-, which gradually penetrates the corrosion product layer and forms soluble chloride ($MgCl_2$ + $Mg_x(OH)_yCl_z$), destroying the protective effect of the corrosion product layer[14-27]. The surface of the fresh magnesium alloy is again exposed to the aqueous solution, the open circuit potential shifts negatively, the dissolution rate accelerates, and the corrosion product layer re-forms on the surface, causing the open circuit potential to fluctuate around a certain value. The greater the fluctuation, the worse is the stability of the surface layer[18-30]. The open circuit potentials are high, and they thermodynamically show that the addition of rare earth Sm can improve the stability of the surface layer on Mg-5Y-2Nd-*x*Sm-0.5Zr magnesium alloys. However, excess rare earth Sm causes the alloys to have negative potentials and decreases the thermal stability[19-31].

3.4.2 Dynamic polarization curve

Fig. 7 shows the effects of Sm content on the polarization curve of Mg-5Y-2Nd-*x*Sm-0.5Zr alloys. According to the Tafel formula (4)[17-33]:

$$\Delta E_k = -B_k \lg(i_k / i_c) \quad (4)$$

The corrosion potential E_{corr} is extrapolated in the Tafel area, and the corrosion current density I_{corr} is obtained. The results are shown in Table 3. Fig. 7 shows that the cathode hydrogen evolution reaction curves of the alloys are basically the same, indicating that adding Sm has little effect on the cathode reaction.

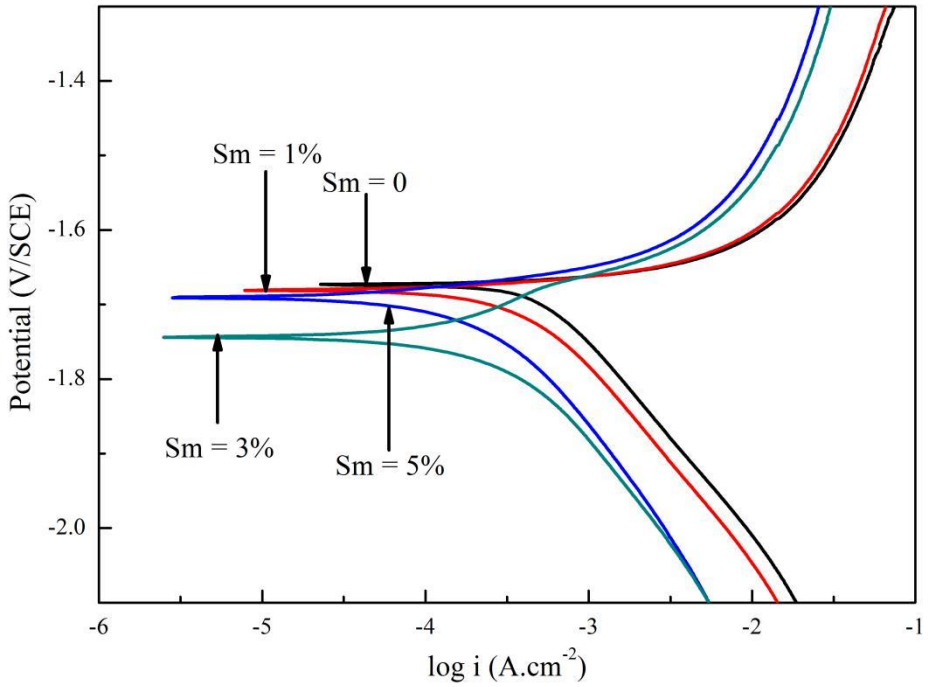

Figure 7. Polarization curves for peak-aged Mg-5Y-2Nd-*x*Sm-0.5Zr alloys (*x*=0, 1, 3, 5) (wt.%).

However, on the anode branch, the corrosion current densities of the alloys with Sm are lower than that of the Mg-5Y-2Nd-0.5Zr alloy at the same potential. These lower current densities indicate

that the corrosion rate of the Mg-5Y-2Nd-*x*Sm-0.5Zr series alloys is lower than that of the original alloy at the same potential and that the addition of Sm has a protective effect on the passivating film on the surface of the alloy. As shown in Table 3, the self-corrosion current densities of the alloys with Sm are lower than that of the Mg-5Y-2Nd-0.5Zr alloy. The corrosion rate of an alloy is proportional to its self-corrosion current density, which also reflects the lower corrosion rate of the alloys with Sm. However, excessive Sm causes the uneven second phase distribution in the alloy, which reduces the compactness of the alloy surface film, resulting in a decrease in the local corrosion resistance of the passivating film on the alloy surface[16-34]. As shown in Table 3, when the corrosion resistance of an alloy is increased or a corrosion inhibitor is added, the Tafel slopes of the anode and cathode are larger. By comparison, the B_c and B_a of the Mg-5Y-2Nd-3Sm-0.5Zr alloy are significantly greater than those of the other alloys. In summary, the Mg-5Y-2Nd-3Sm-0.5Zr alloy has the best corrosion resistance of the alloys tested.

Table 3. Specific values for Mg-5Y-2Nd-*x*Sm-0.5Zr alloys (*x*=0, 1, 3, 5) (wt.%) derived from polarization curves.

Samples	B_a (mV/decade)	B_c (mV/decade)	I_{corr} (A.cm^{-2})	E_{corr} (V)
Mg-5Y-2Nd-0.5Zr	58.17	42.71	2.671×10^{-3}	-1.673
Mg-5Y-2Nd-**1Sm**-0.5Zr	64.21	48.41	9.254×10^{-4}	-1.681
Mg-5Y-2Nd-**3Sm**-0.5Zr	115.65	53.66	1.396×10^{-4}	-1.744
Mg-5Y-2Nd-**5Sm**-0.5Zr	73.44	52.56	2.062×10^{-4}	-1.691

3.4.3 AC impedance test

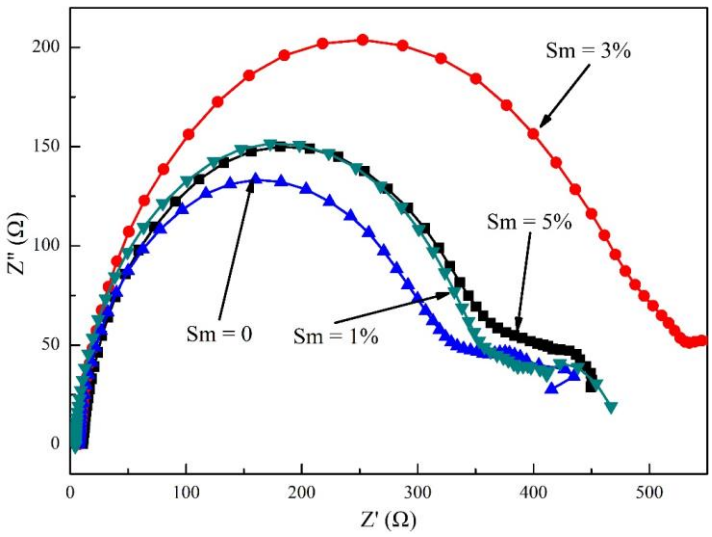

Figure 8. EIS spectra of peak-aged Mg-5Y-2Nd-*x*Sm-0.5Zr alloys (*x*=0, 1, 3, 5) (wt.%).

To study the effects of Sm on the corrosion resistance of Mg-5Y-2Nd-*x*Sm-0.5Zr magnesium alloys, impedance analysis was carried out on the Mg-5Y-2Nd-*x*Sm-0.5Zr alloys in 3.5% NaCl solution. The Nyquist diagrams are shown in Figure 8. Fig. 8 shows that in 3.5 wt.% NaCl solution, the impedance spectra of the Sm-containing and Sm-free magnesium alloys are similar in shape, and all have a high-frequency capacitive anti-arc and a low-frequency capacitive anti-arc. Each high-frequency capacitive arc is due to the electric double layer generated by the Mg substrate and the solution interface. Each medium-low-frequency capacitive arc is mainly due to the mass transfer process in the corrosion product layer on the alloy surface[19-29]. Many magnesium alloy researchers study the Nyquist curves of different magnesium alloys. It is believed that the larger the radius of the high-frequency capacitive arc, the lower is the corrosion rate of the alloy, that is, the better the corrosion resistance[9-34]. Therefore, when the alloy Sm content is 3 wt.%, the corrosion resistance of the alloy tends to be optimal in the same corrosive environment; this result is consistent with the weight loss corrosion results.

Based on the shape of Nyquist and Bode plots, the equivalent circuit is shown in Figure 9, where R_s is the solution resistance, R_t is the charge transfer resistance, *CPE* is the constant phase angle element. Table 4 shows the equivalent circuit parameters for the experimental alloys after software fitting. Analysis of the data in Table 4 shows that the R_s values for all the alloys are very small, indicating that the solution resistance has little effect on the experimental process and can be ignored. The R_t of Mg-5Y-2Nd-3Sm-0.5Zr alloy is greatly improved compared with other alloys, while its *CPE* is significantly reduced. Mg-5Y-2Nd-3Sm-0.5Zr alloy also has a high inductive value, indicating that adding 3% Sm can effectively improve the surface condition of the Mg-Y-Nd-Sm alloy reduces the corrosion tendency of the alloy and hinders the transfer of charge at the interface between the electrode and the electrolyte solution, thereby hindering the progress of the electrode process and improving the corrosion resistance of the alloy.

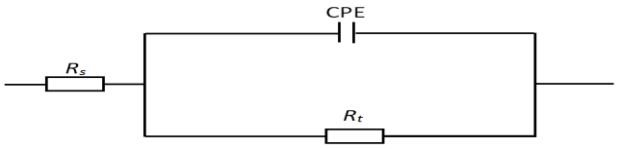

Figure 9. Equivalent circuit of EIS for the Mg-5Y-2Nd-*x*Sm-0.5Zr (*x*=0, 1, 3, 5) (wt.%) alloys.

Table 4. Fitting results of the EIS of the Mg-5Y-2Nd-*x*Sm-0.5Zr (*x*=0, 1, 3, 5) (wt.%) alloys.

Samples	*Rs*/ $\Omega \cdot cm^2$	*CPE*/ $\times 10^{-5} \mu F \cdot cm^{-2}$	*n*	*Rt*/ $\Omega \cdot cm^2$
Mg-5Y-2Nd-0.5Zr	9.088	2.897	0.8860	360.2
Mg-5Y-2Nd-**1Sm**-0.5Zr	8.896	2.767	0.8849	383.9
Mg-5Y-2Nd-**3Sm**-0.5Zr	8.987	1.887	0.8986	524.1
Mg-5Y-2Nd-**5Sm**-0.5Zr	9.269	2.165	0.9267	396.6

3.5 Corrosion Mechanism.

When the alloy is in air, it forms a layer of MgO. When the magnesium alloy is immersed in NaCl solution, the oxide film layer has a certain corrosion resistance at positions protected by the oxide film, thereby protecting the magnesium matrix, but the protective effect is weak, and the oxide film is gradually dissolved. The reaction is shown in formula (5)[19-35]:

$MgO+H_2O \rightarrow Mg(OH)_2$ (5)

In sodium chloride solution, Cl^- adsorbed on the surface of the material can convert part of the $Mg(OH)_2$ into $MgCl_2$, which is soluble in water, causing the oxide film on the surface of the magnesium alloy to rupture and stop protecting the matrix. Therefore, the magnesium matrix is directly exposed to the NaCl solution, and the reaction is shown by formulas (6-9)[11-35]:

Anodic reaction: $Mg \rightarrow Mg^+ + e^-$ (6)

$2Mg^+ + 2H_2O \rightarrow 2Mg^{2+} + 2OH^- + H_2\uparrow$ (7)

Cathodic reaction: $2H_2O + 2e^- \rightarrow H_2\uparrow + 2OH^-$ (8)

Total reaction: $Mg + 2H_2O \rightarrow Mg(OH)_2 + H_2\uparrow$ (9)

The magnesium matrix dissolves as an anode, forming the corrosion product $Mg(OH)_2$, which further enters the corrosion pit. The Cl^- continues to convert the $Mg(OH)_2$ into soluble $MgCl_2$, which re-exposes the magnesium matrix to the corrosive medium. The pits are deepened and their size increases, eventually forming localized corrosion and even overall corrosion. At places not protected by the oxide film, the Mg-5Y-2Nd-*x*Sm-0.5Zr alloy matrix directly contacts the NaCl solution and dissolution of magnesium and reduction of water occur as shown in formulas (5-9). Second phases and impurities easily form at grain boundaries, which are sensitive areas where corrosion occurs. The number, morphology and distribution state of precipitated phase particles in an aged alloy determine whether these particles play a role in improving the corrosion resistance of the alloy. When the number of precipitated phases is high, the particles are fine, and the particles are dispersed in the matrix, the corrosion resistance of the rare earth-containing precipitates is improved, and the dispersion is distributed on the substrate around the corrosion pit, which promotes the expansion and extension of the corrosion pit to a certain extent. The blocking effects improve the corrosion resistance of the alloy. When the number of precipitated phases is small, the particles are coarse and segregated in the matrix; since the potential of the rare earth compound is more positive than that of the α-Mg matrix, galvanic corrosion of the matrix easily forms, which increases the corrosion rate of the magnesium alloy and weakens its corrosion resistance[14-36].

4. CONCLUSION

(1) With increasing Sm content, the large, coarse second phase in the alloy disappeared. A new, fine grained secondary phase appeared in the alloy, and its distribution was relatively uniform. The alloy structure was mainly composed of α-Mg, $Mg_{24}Y_5$, $Mg_{41}Nd_5$ and $Mg_{41}Sm_5$ phases.

(2) A proper addition of Sm can improve the amount of second phases in the Mg-5Y-2Nd-0.5Zr alloy and make the microstructure and composition more uniform. The uniform, fine second

phases can prevent corrosion and increase corrosion resistance.

(3) With the addition of rare earth Sm (0 wt.% - 5 wt.%), the corrosion rate of 3.5 wt.% NaCl solution first decreased and then increased, reaching a minimum at 3 wt.% Sm content.

(4) The open circuit potentials and polarization curves of the alloys showed that the corrosion rate is related to the Sm content in the alloy. A proper amount of Sm can positively shift the open circuit potential of the Mg-5Y-2Nd-0.5Zr alloy, decrease the corrosion current density, and improve the corrosion resistance; similar conclusions were also reached through AC impedance analysis.

ACKNOWLEDGMENTS
This work was supported by the National Natural Science Foundation of China (Nos 51571084 and 51171059), and Henan Province Key Scientific and Technological Projects (Nos 152102210072).

CONFLICTS OF INTEREST
We declare that we do not have any commercial or associative interest that represents a conflict of interest in connection with the work submitted.

References

1. B.L. Mordike, T. Ebert, *Mat. Sci. Eng. A-Struct.*, 302 (2001) 37.
2. C.Y. Su, D.J. Li, A.A. Luo, T. Ying and X.Q. Zeng, *J. Alloy. Compd.*, 747 (2018) 431.
3. Y. Fan, G. Wu, H. Gao, G. Li and C. Zhai, *J. Mater. Sci.*, 41 (2006) 409.
4. Y. Song, D. Shan, R. Chen and E.H. Han, *Corros. Sci.*, 52 (2010) 1830.
5. S. Pawar, T.J.A. Slater, T.L. Burnett, X. Zhou, G.M. Scamans, Z. Fan, G.E. Thompson, P.J. Withers, *Acta. Mater.*, 133 (2017) 90.
6. S. Schumann, H.E. Friedrich , *Mater. Sci. Forum*, 419 (2003) 51.
7. J.D. Robson, S.J. Haigh, B. Davis and D. Griffiths, *Metall. Mater. Trans. A*, 47 (2016) 522.
8. T. Takenaka, T. Ono, Y. Narazaki, Y. Naka, M. Kawakami, *Acta,* 53 (2007) 117.
9. S.Y. Xie, X.D. Peng, J.C. Li, C.G. Wang and Y. Yang, *Rare. Metal. Mat. Eng.*, 43 (2014) 52.
10. N. Birbilis, M.A. Easton, A.D. Sudholz, S.M. Zhu and M.A. Gibson, *Corros. Sci.*, 51 (2009) 683.
11. L.L. Rokhlin, T.V. Dobatkina, N.I. Nikitina, *Mater. Sci. Forum*, 419 (2003) 291.
12. O. Lunder, J.E. Lein, T.K. Aune and K. Nisancioglu, *Corrosion*, 45 (2012) 741.
13. E. Aghion, B. Bronfin, F.V. Buch, S. Schumann and H. Friedrich, *JOM*, 55 (2003) 30.
14. L. Shi, D.O. Northwood, *Acta. Metall. Sin.*, 42 (1994) 871.
15. D.Q. Li, Q.D. Wang and W.J. Ding, *Mat. Sci. Eng. A-Struct.*, 448 (2007) 165.
16. [S.W. Nam, W.T. Kim, D.H. Kim and T.S. Kim, *Met. Mater. Int.*, 19 (2013) 205.
17. B.J. Wang, D.K. Xu, J.H. Dong, W. Ke, *Scr. Mater.*, 88 (2014) 5.
18. R. Arrabal, A. Pardo, M.C. Merino, M. Mohedano and P. Casajús, *Corros. Sci.*, 55 (2012) 301.
19. M. Sun, G. Wu, W. Wang and W. Ding, *Mat. Sci. Eng. A-Struct.*, 523 (2009) 145.
20. Y.W. Gui, Q.A. Li and J. Chen, *Mater. Res. Express*, 5 (2018) 7.
21. O Zheng, J.P. Zhou, D.S. Zhao, J.B. Wang and R.H. Wang, *Scripta. Mater.*, 60 (2009) 791.
22. H. Qiu, H. Yan and Z. Hu, *J. Alloy. Compd.*, 567 (2013) 77.
23. Q.A. Li, X.F. Li, Q. Zhang and J. Chen, *Rare. Metals*, 29 (2010) 557.
24. Y. Zhang, C. Yan, F. Wang and W. Li, *Corros. Sci.*, 47 (2005) 2816.
25. J.F. Nie, B.C. Muddle, *Acta. Mater.*, 48 (2000) 1691.
26. S.J. Xia, R. Yue, R.G. Rateick and V.I. Birss, *J. Electrochem. Soc.*, 15l (2004) 179.
27. G.L. Song, A. Atrens, *Adv. Eng. Mater.*, 1(1999) 11.
28. J. Li, Q. Jiang, H. Sun and Y. Li, *Corros. Sci.*, 111 (2016) 288.
29. W.L. Ren, Q.A Li, J.H. Li, K.J. Li and X.Y. Zhang, *China. Foundry*, 117 (2010) 262.
30. J. Chen, Q.A. Li, J.H. Li, X.F. Li, K.J. Li and X.Y. Zhang, *China. Foundry*, 6 (2009) 124.

31. K.J. Li, Q.A Li, X.T Jing, J. Chen, X.Y. Zhang and Q. Zhang, *Scripta. Mater.*, 60 (2009) 1101.
32. L.L. Rokhlin, N.I. Nikitina, *Phys. Met. Metallogr.*, 82 (1996) 113.
33. H.R.J. Nodooshan, W.C. Liu, G.H. Wu, Y. Rao, C.X. Zhou, S.P. He, W.J. Ding and R. Mahmudi, *Mat. Sci. Eng. A-Struct.*, 615 (2014) 79.
34. C. Liu, J. Liang, J. Zhou, L. Wang and Q. Li, *Appl. Surf. Sci.*, 343 (2015) 133.
35. J. Zhou, J. Xu, S. Huang, Z. Hu and X. Meng, *Surf. Coat. Tech.*, 309 (2016) 212.
36. B.J. O'Brien , W.M. Carroll, A.J. Conneely and G.M. O'Connor, *P. I. Mech. Eng. C-J. Mec.*, 228 (2013) 278.